Anisotropy and Corotation of Galactic Cosmic Rays
M. Amenomori, *et al.*
Science **314**, 439 (2006);
DOI: 10.1126/science.1131702

7. D. Gottesman, thesis, California Institute of Technology, Pasadena, CA (1997).
8. D. Gottesman, *Phys. Rev. A* **57**, 127 (1998).
9. M. A. Nielsen, I. L. Chuang, *Quantum Computation and Quantum Information* (Cambridge Univ. Press, New York, 2000).
10. A. M. Steane, *Phys. Rev. Lett.* **77**, 793 (1996).
11. A. R. Calderbank, P. W. Shor, *Phys. Rev. A* **54**, 1098 (1996).
12. D. J. C. MacKay, G. Mitchison, P. L. McFadden, *IEEE Trans. Inf. Theory* **50**, 2315 (2004).
13. D. Fattal, T. S. Cubitt, Y. Yamamoto, S. Bravyi, I. L. Chuang, Entanglement in the stabilizer formalism (2004). Available at http://arxiv.org/abs/quant-ph/0406168.
14. S. Bravyi, D. Fattal, D. Gottesman, *J. Math. Phys.* **47**, 062106 (2006).
15. G. Bowen, *Phys. Rev. A* **66**, 052313 (2002).
16. A. R. Calderbank, E. M. Rains, P. W. Shor, N. J. A. Sloane, *IEEE Trans. Inf. Theory* **44**, 1369 (1998).
17. Proofs and the detailed construction are available as supporting material on *Science* Online.
18. C. H. Bennett, P. W. Shor, J. A. Smolin, A. Thapliyal, *IEEE Trans. Inf. Theory* **48**, 2637 (2002).
19. I. Devetak, A. W. Harrow, A. J. Winter, *Phys. Rev. Lett.* **93**, 230504 (2004).
20. C. Berrou, A. Glavieux, P. Thitimajshima, *Proceedings of the IEEE International Conference on Communications (ICC '93)*, Geneva, Switzerland, May 1993 (IEEE, New York, 1993), pp. 1064–1070 (1993).
21. R. G. Gallager, thesis, Massachusetts Institute of Technology, Cambridge, MA (1963).
22. E. Knill, R. Laflamme, *Phys. Rev. A* **55**, 900 (1997).
23. C. H. Bennett, D. P. DiVincenzo, J. A. Smolin, W. K. Wooters, *Phys. Rev. A* **54**, 3824 (1996).

24. We acknowledge helpful feedback from D. Poulin, G. Smith, and J. Yard. T.A.B. acknowledges financial support from NSF grant no. CCF-0448658, and T.A.B. and M.H.H. both received support from NSF grant no. ECS-0507270. I.D. and M.H.H. acknowledge financial support from NSF grant no. CCF-0524811 and NSF grant no. CCF-0545845.

Supporting Online Material
www.sciencemag.org/cgi/content/full/1131563/DC1
SOM Text

20 June 2006; accepted 31 August 2006
Published online 28 September 2006;
10.1126/science.1131563
Include this information when citing this paper.

Anisotropy and Corotation of Galactic Cosmic Rays

M. Amenomori,[1] S. Ayabe,[2] X. J. Bi,[3] D. Chen,[4] S. W. Cui,[5] Danzengluobu,[6] L. K. Ding,[3] X. H. Ding,[6] C. F. Feng,[7] Zhaoyang Feng,[3] Z. Y. Feng,[8] X. Y. Gao,[9] Q. X. Geng,[9] H. W. Guo,[6] H. H. He,[3] M. He,[7] K. Hibino,[10] N. Hotta,[11] Haibing Hu,[6] H. B. Hu,[3] J. Huang,[12] Q. Huang,[8] H. Y. Jia,[8] F. Kajino,[13] K. Kasahara,[14] Y. Katayose,[4] C. Kato,[15] K. Kawata,[12] Labaciren,[6] G. M. Le,[16] A. F. Li,[7] J. Y. Li,[7] Y.-Q. Lou,[17] H. Lu,[3] S. L. Lu,[3] X. R. Meng,[6] K. Mizutani,[2,18] J. Mu,[9] K. Munakata,[15] A. Nagai,[19] H. Nanjo,[1] M. Nishizawa,[20] M. Ohnishi,[12] I. Ohta,[21] H. Onuma,[2] T. Ouchi,[10] S. Ozawa,[12] J. R. Ren,[3] T. Saito,[22] T. Y. Saito,[12] M. Sakata,[13] T. K. Sako,[12] T. Sasaki,[10] M. Shibata,[4] A. Shiomi,[12] T. Shirai,[10] H. Sugimoto,[23] M. Takita,[12] Y. H. Tan,[3] N. Tateyama,[10] S. Torii,[18] H. Tsuchiya,[24] S. Udo,[12] B. Wang,[9] H. Wang,[3] X. Wang,[12] Y. G. Wang,[7] H. R. Wu,[3] L. Xue,[7] Y. Yamamoto,[13] C. T. Yan,[12] X. C. Yang,[9] S. Yasue,[25] Z. H. Ye,[16] G. C. Yu,[8] A. F. Yuan,[6] T. Yuda,[10] H. M. Zhang,[3] J. L. Zhang,[3] N. J. Zhang,[7] X. Y. Zhang,[7] Y. Zhang,[3] Yi Zhang,[3]* Zhaxisangzhu,[6] X. X. Zhou[8] (The Tibet ASγ Collaboration)

The intensity of Galactic cosmic rays is nearly isotropic because of the influence of magnetic fields in the Milky Way. Here, we present two-dimensional high-precision anisotropy measurement for energies from a few to several hundred teraelectronvolts (TeV), using the large data sample of the Tibet Air Shower Arrays. Besides revealing finer details of the known anisotropies, a new component of Galactic cosmic ray anisotropy in sidereal time is uncovered around the Cygnus region direction. For cosmic-ray energies up to a few hundred TeV, all components of anisotropies fade away, showing a corotation of Galactic cosmic rays with the local Galactic magnetic environment. These results have broad implications for a comprehensive understanding of cosmic rays, supernovae, magnetic fields, and heliospheric and Galactic dynamic environments.

The anisotropy of Galactic cosmic rays (GCRs) may result from an uneven distribution of cosmic ray (CR) sources and the process of CR propagation in the Milky Way. CRs with energy below 10^{15} eV are accelerated by diffusive magnetohydrodynamic (MHD) shocks (*1*–*4*) of supernova remnants (SNRs) and stellar winds. The discreteness of SNRs might lead to a CR anisotropy (*5*). However, in reality, GCRs must almost completely lose their original directional information; their orbits are deflected by the Galactic magnetic field (GMF) and are randomized by irregular GMF components, having traveled on average for many millions of years, some also having interacted with interstellar gas atoms and dust. The transport of CRs in a magnetized plasma is governed by four major processes: convection, drift, anisotropic diffusion, and adiabatic energy change (deceleration or acceleration) (*6*, *7*). High-precision measurement of the CR anisotropy provides a means to explore magnetic field structures and provides insight for the CR transport parameters (*8*). The long-term high-altitude observation at the Tibet Air Shower Arrays (referred to as the Tibet ASγ experiment) has accumulated tens of billions of CR events in the multi-TeV energy range, ready for an unprecedented high-precision measurement of the CR anisotropy as well as the temporal and energy dependence of the CR anisotropy.

An expected anisotropy is caused by the relative motion between the observer and the CR plasma, known as the Compton-Getting (CG) effect (*9*), with CRs of greater intensity arriving from the direction of motion and those of less intensity arriving from the opposite direction. Such a CR anisotropy, caused by Earth's orbital motion around the Sun, has indeed been detected (*10*, *11*). Data assembled up until the 1930s (*9*) were consistent with a scenario that the CR plasma stays at rest in an inertial frame of reference attached to the Galactic center. If this were true, the Galactic rotation in the solar neighborhood might then be measurable. Nevertheless, such CR anisotropy due to the solar system rotation around the Galactic center at a speed of ~220 km s^{-1} remained inconclusive for more than seven decades. Now our high-precision two-dimensional (2D) measurement gives strong evidence for excluding the CR anisotropy of this origin and thus show a corotation of GCRs with the local GMF environment.

Historically, the GCR anisotropy (*12*, *13*) has been measured as the sidereal time variation at the spinning Earth, using both underground μ detectors and ground-based air shower arrays (*14*–*19*). Located at different geographic latitudes and operating in different years with various threshold energies, each individual experiment could only measure the CR

[1]Department of Physics, Hirosaki University, Hirosaki 036-8561, Japan. [2]Department of Physics, Saitama University, Saitama 338-8570, Japan. [3]Key Laboratory of Particle Astrophysics, Institute of High Energy Physics, Chinese Academy of Sciences, Beijing 100049, China. [4]Faculty of Engineering, Yokohama National University, Yokohama 240-8501, Japan. [5]Department of Physics, Hebei Normal University, Shijiazhuang 050016, China. [6]Department of Mathematics and Physics, Tibet University, Lhasa 850000, China. [7]Department of Physics, Shandong University, Jinan 250100, China. [8]Institute of Modern Physics, SouthWest Jiaotong University, Chengdu 610031, China. [9]Department of Physics, Yunnan University, Kunming 650091, China. [10]Faculty of Engineering, Kanagawa University, Yokohama 221-8686, Japan. [11]Faculty of Education, Utsunomiya University, Utsunomiya 321-8505, Japan. [12]Institute for Cosmic Ray Research, University of Tokyo, Kashiwa 277-8582, Japan. [13]Department of Physics, Konan University, Kobe 658-8501, Japan. [14]Faculty of Systems Engineering, Shibaura Institute of Technology, Saitama 337-8570, Japan. [15]Department of Physics, Shinshu University, Matsumoto 390-8621, Japan. [16]Center of Space Science and Application Research, Chinese Academy of Sciences, Beijing 100080, China. [17]Physics Department and Tsinghua Center for Astrophysics, Tsinghua University, Beijing 100084, China. [18]Advanced Research Institute for Science and Engineering, Waseda University, Tokyo 169-8555, Japan. [19]Advanced Media Network Center, Utsunomiya University, Utsunomiya 321-8585, Japan. [20]National Institute of Informatics, Tokyo 101-8430, Japan. [21]Tochigi Study Center, University of the Air, Utsunomiya 321-0943, Japan. [22]Tokyo Metropolitan College of Industrial Technology, Tokyo 116-8523, Japan. [23]Shonan Institute of Technology, Fujisawa 251-8511, Japan. [24]RIKEN, Wako 351-0198, Japan. [25]School of General Education, Shinshu University, Matsumoto 390-8621, Japan.

*To whom correspondence should be addressed. E-mail: zhangyi@mail.ihep.ac.cn

modulation profile along the right ascension (R.A.) direction, which was usually fitted by the first few harmonics. Instead of using sine or cosine harmonics, one may introduce two Gaussian functions with declination (Dec)–dependent parameters (mean, width, and amplitude) to fit the so-called "tail-in" and "loss-cone" features and to obtain a tentative 2D anisotropic picture (*20*, *21*) by simultaneously fitting different experimental data. The CR deficiency was thought to be associated with a magnetic conelike structure and was thus named "loss-cone," whereas the CR enhancement is roughly in the direction of the heliospheric magnetotail and is thus referred to as "tail-in" enhancement (*12*, *13*). However, the spatial and energy dependence of CR anisotropy could not be determined accurately (*22*), and some subtle features remain hard to detect because the CR anisotropy appears more complex and cannot be properly described by two Gaussian functions. The Tibet AS-γ experiment alone can achieve 2D measurement in various energy ranges and can provide details of the 2D CR anisotropy.

The Tibet Air Shower Array experiment. The Tibet Air Shower Array experiment has been conducted at Yangbajing (90.522 E, 30.102 N; 4300 m above sea level) in Tibet, China, since 1990. In 1994, the Tibet I array (*23*)—consisting of 49 scintillation counters and forming a 7 by 7 matrix with a 15-m span—was expanded to become the Tibet II array, with an area of 36,900 m^2, by increasing the number of counters. In 1996, part of Tibet II with an area of 5175 m^2 was upgraded to a high-density (HD) array with a 7.5-m span (*24*). To increase the event rate, the HD array was enlarged in 1999 to cover the central part of the Tibet II array and became the Tibet III array (*25*–*27*). The area of the Tibet III array has reached 22,050 m^2. The trigger rates are ~105 Hz and ~680 Hz for the Tibet HD and III arrays, respectively. The data were acquired by running the HD array for 555.9 live days (the cumulative time when the array is waiting for selection of new CR events) from February 1997 to September 1999 and the Tibet III array for 1318.9 live days from November 1999 to October 2005. GCR events are selected for inclusion if any four-fold coincidence occurs in the counters with each recording more than 0.8 particles in charge, if the air shower core position is located in the array, and if the zenith angle of arrival direction is ≤40°. With all those criteria, both Tibet HD and III arrays have the modal energy of 3 TeV and a moderate energy resolution; the ~0.9° angular resolution estimated from Monte Carlo simulations (*28*, *29*) was verified by measuring the Moon shadow of CRs (*25*–*27*). In total, ~37 billion CR events are used in our data analysis.

Data analysis and results. With such a large data sample, we conducted a 2D measurement to reveal detailed structural information of the large-scale GCR anisotropy beyond the simple R.A. profiles. For each short time step (e.g., 2 min), the relative CR intensity at points in each zenith angle belt can be compared, and this comparison can be extended step by step to all points in the surveyed sky [see (*30*) for details of data analysis]. Lacking the absolute detector efficiency calibration in the Dec direction, absolute CR intensities along different Dec directions cannot be compared. Thus, the average intensity in each narrow Dec belt is normalized to unity. Our analysis procedure would give a correct 2D anisotropy if there is no variation in the average CR intensity for different Dec. We systematically examined the CR anisotropy in four different time frames: solar time for solar modulation, sidereal time for Galactic modulation, antisidereal time, and extended-sidereal time for systematic studies; we found systematic variations to be unimportant because CR intensity variations of the latter two (not shown) are not consistent with statistical fluctuations.

To study the temporal variation of CR modulation, we divided the data sample into two subsets. The first subset is from February 1997 to October 2001, covering the 23rd solar maximum (a period of a few years when solar magnetic activity is strongest); the second subset is from December 2001 to November 2005, approaching the solar minimum (a period of a few years when solar magnetic activity becomes minimal). Comparing the sidereal time plots for these two intervals (Fig. 1, A to C) shows that the CR anisotropy is fairly stable and insensitive to solar activity. The tail-in and loss-cone anisotropy components (*12*, *13*), extracted earlier from a combination of the underground μ telescope data analyses (*20*, *21*), are seen in our 2D plots in much finer detail and with a high accuracy (Fig. 1, A and B). Our new high-

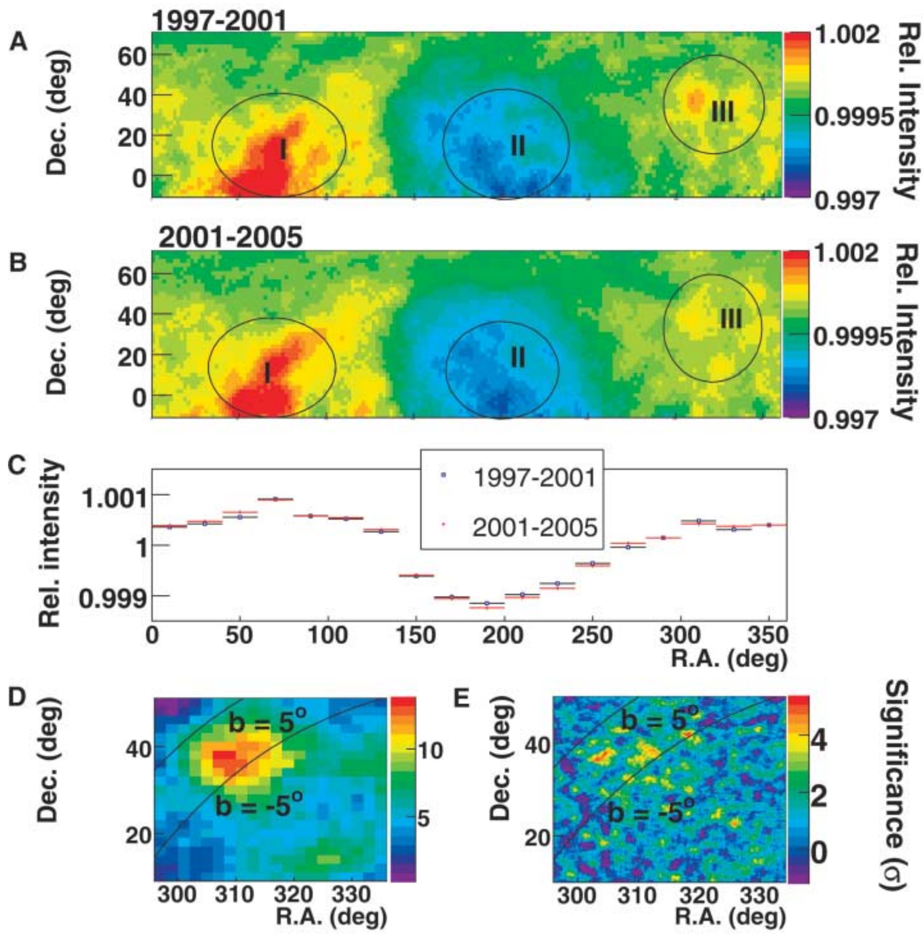

Fig. 1. Celestial CR intensity map for Tibet ASγ data taken from (**A**) 1997 to 2001 and (**B**) 2001 to 2005 (*40*). The vertical color bin width is 2.5×10^{-4} for the relative intensity in both (A) and (B). The circled regions labeled by I, II, and III are the tail-in component, the loss-cone component (*12*, *13*), and the newly found anisotropy component around the Cygnus region (~38°N Dec and ~309° R.A.), respectively. (**C**) The 1D projection of the 2D maps in R.A. for comparison. (**D**) and (**E**) show significance maps of the Cygnus region [pixels in radius of 0.9° and sampled over a square grid of side width 0.25° for (E)] for data from 1997 to 2005. The vertical color bin widths are 0.69 SD and 0.42 SD for significance in (D) and (E), respectively. Two thin curves in (D) and (E) stand for the Galactic parallel $b = \pm5°$. Small-scale anisotropies (E) superposed onto the large-scale anisotropy hint at the extended gamma-ray emission.

precision measurement thus provides constraints on physical interpretations of these features.

Spreading across ~280° to ~360° in R.A., a new excess component with a ~0.1% increase of the CR intensity that peaks at Dec ~38°N and R.A. ~309° in the Cygnus region is detected at a significance level of 13.3 SD with a 5° pixel radius (Fig. 1D). The Cygnus region, where complex features are revealed in broad wavelength bands of radio, infrared, x-rays, and gamma rays, is rich in candidate GCR sources. Recently, the first unidentified TeV gamma-ray source was discovered here by high-energy gamma-ray astronomy experiment (HEGRA) (*31*). This region, as observed by energetic gamma-ray experiment telescope (EGRET) (*32*), appears to be the brightest source of diffuse GeV gamma rays in the northern sky and contributes substantially to the diffuse TeV gamma-ray emission in the Galactic plane as observed by Milagro (*33*), which rejects 90% of CR background while retaining ~45% of gamma rays. Such gamma rays originate from the interaction of CRs with gas and dust. Using more stringent event selection criteria (*30*), a deeper view of the Cygnus region with a 0.9° pixel radius shows that the large-scale excess consists of a few spatially separated enhancements of smaller scale superposed onto a large-scale anisotropy (Fig. 1E); this small-scale (~2°) excess favors the interpretation that the extended gamma-ray emission from the Cygnus region contributes considerably to the overall excess in the region (*34*). Because our experiment cannot yet distinguish gamma rays from the charged CR background, we cannot tell how much of this excess can be attributed to gamma rays and how much, if any, is associated with charged CRs (*35*). Such a determination requires upgrading the Tibet Air Shower arrays for CR and gamma-ray discrimination.

The solar time CR modulation was also stable (Fig. 2). We found that including events with fewer than eight detector coincidences (lower energy events) resulted in much larger modulation amplitudes than those obtained when these events were excluded (higher energy events). To avoid this, high multiplicity events with coincident detector numbers ≥8 were adopted (Fig. 2). The observed dipole anisotropy agrees very well with the expected CG effect as a result of Earth's orbital motion around the Sun. Thus, heliospheric magnetic field and solar activity does not influence the multi-TeV CR anisotropy.

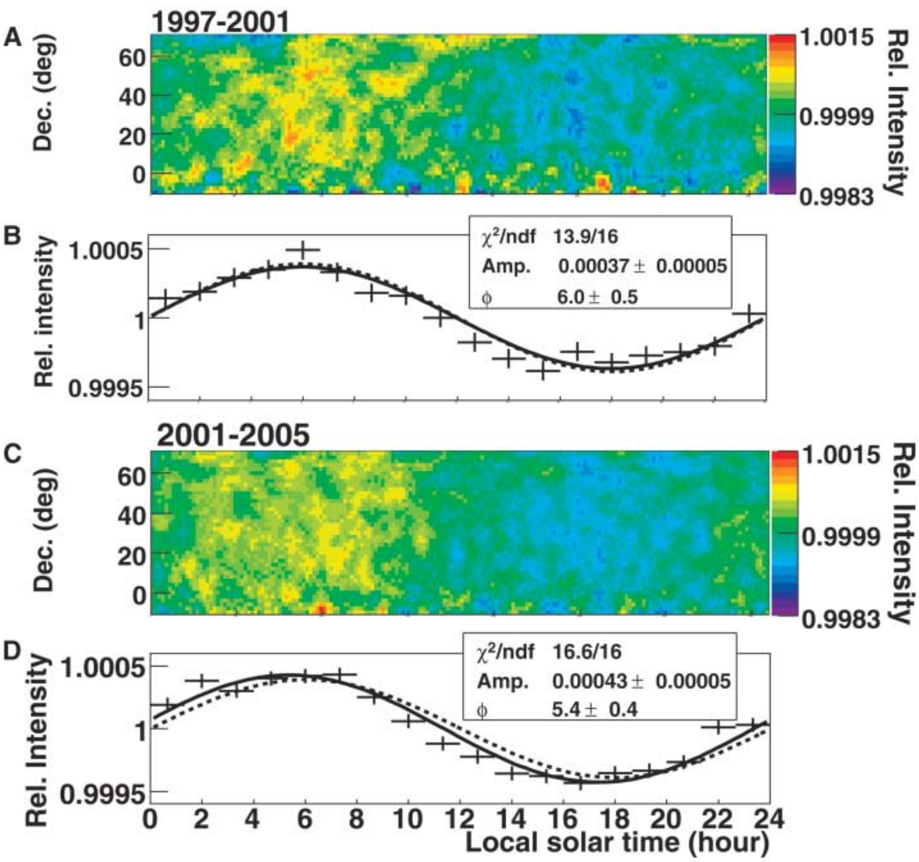

Fig. 2. Local solar time CR intensity map for the Tibet ASγ data taken from (**A** and **B**) 1997 to 2001 and (**C** and **D**) 2001 to 2005. Both samples have the modal energy of 10 TeV. The vertical color bin is 1.6×10^{-4} for the relative intensity in (A) and (C). In (B) and (D), the fitting function is in the form of Amp $\times$ $\cos[2\pi(T - \phi)/24]$, where the local solar time T and ϕ are in units of hours and Amp is the amplitude. The χ^2 fit involves the number of degrees of freedom (ndf) given by the number of bins minus two, due to the two fitting parameters Amp and ϕ. The 1D plots are projections of the 2D maps in local solar time. In the 1D plots, the dashed lines are from the expected CG effect and the solid lines are the best harmonic fits, which agree well with the prediction. The solar time modulation appears stable and insensitive to solar activity.

Because of the stable nature of the sidereal time modulation, data from different years were combined to examine the energy dependence of CR anisotropy. Figure 3 shows the variation of anisotropy for five groups of events according to their different primary energies. For primary energies below 12 TeV, the anisotropies show little dependence on energy, whereas above this level, anisotropies fade away, consistent with a CR isotropy of Karlsruhe Shower Core and Array Detector (KASCADE) (*17*) in the energy range of 0.7 to 6 petaelectronvolts (PeV). Contrary to the earlier suggestion (*13*), the tail-in component remains visible above 50 TeV in smaller regions. Because the multi-TeV GCRs, whose gyroradii are hundreds or thousands of astronomical units, are not affected by the heliospheric magnetic field, it is clear that the GMF must be responsible for both tail-in and loss-cone modulations.

As a result of diminishing GCR anisotropy at high energies, we can test the CG anisotropy caused by the orbital motion of the solar system around the Galactic center, which would peak at α (R.A.) = 315°, δ (Dec) = 49° and minimize at α = 135°, δ = –49°, with an amplitude of 0.35%. This would be a salient signal in a real 2D measurement. However, as explained earlier, the modulation along the Dec direction is partly lost. After applying the normalization procedure along each Dec belt, the expected CG anisotropy is distorted and apparently peaks at α = 315°, δ = 0° and forms a trough at around α = 135°, δ = 0° with a smaller amplitude of ~0.23% (Fig. 4). To avoid any contamination from the nonvanishing tail-in and loss-cone anisotropies (*12*, *13*) when the primary energy is ~300 TeV, the upper half of the surveyed CR intensity map (with Dec > 25°) is used to compare with the predicted Galactic CG effect of amplitude ~0.16%. The fitted anisotropy amplitude is 0.03% ± 0.03%, consistent with an isotropic CR intensity. Therefore, our observations exclude the existence of other unknown Galactic CG effect with a confidence level of ~5 SD, assuming the absence of canceling effects. The null result of the Galactic CG effect implies that GCRs corotate with the local GMF environment.

Discussion. The observation of GCR anisotropy and diffuse gamma-ray emission plays an important role in probing sources and propagation of CRs. The detection of the new large-scale GCR anisotropy component and the indication of extended gamma-ray emission from the same mysterious Cygnus region allow us to connect the GCR acceleration site and propagation. A precise spectral and morphological determination of the extended gamma-ray emission would be our next pursuit. The existence of large-scale GCR anisotropies up to a few tens of TeV indicates that they are not related to the heliospheric magnetic field. It is conceivable that GMF has large-scale structures in the heliospheric neighborhood.

As in many spiral galaxies, the Milky Way has large-scale differential rotations in stellar and magnetized gas disks with a GMF of a few μG. The GMF, GCRs, and thermal gas have similar energy densities of ~1 eV cm^{-3} and interact with each other dynamically. The corotation of the GCR plasma with the local GMF environment around the Galactic center is enforced by the Lorentz force as GCRs randomly scatter and drift in irregular GMF components (*36*). As the Galactic disk rotates differentially, the important inference is that the bulk GCR plasma within and above the Galactic disk must also rotate differentially. The GCR corotation evidence provides an important empirical basis for the study of Galactic MHD processes such as modeling synchrotron emission diagnostics for large-scale spiral structures of MHD density waves (*37*–*39*).

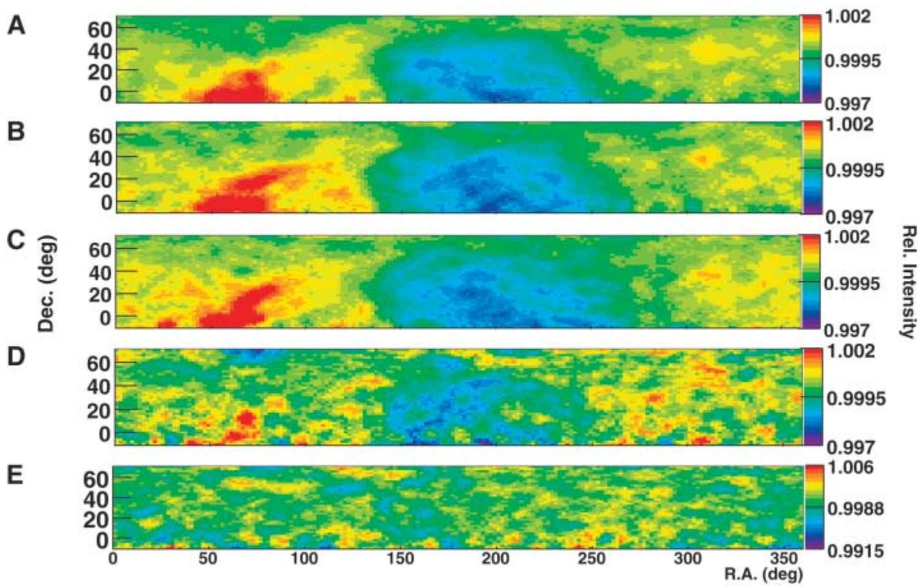

Fig. 3. Celestial CR intensity map for different representative CR energies. (**A**) 4 TeV; (**B**) 6.2 TeV; (**C**) 12 TeV; (**D**) 50 TeV; (**E**) 300 TeV. Data were gathered from 1997 to 2005. The vertical color bin width is 2.5 × 10^{-4} in [(A) to (D)] and 7.25 × 10^{-4} in (E) for different statistics, all for the relative CR intensity.

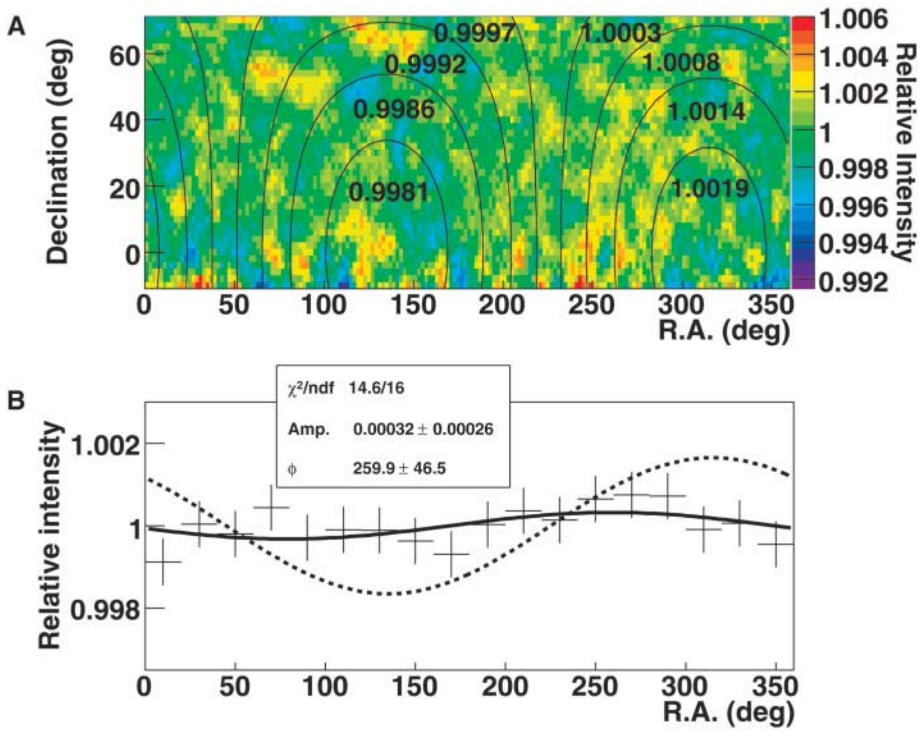

Fig. 4. Celestial or 2D local sidereal time CR intensity map and its 1D projection in the R.A. direction for 300 TeV CRs of all data. (**A**) The colored map is the same as Fig. 3E. The contours are the "apparent" 2D anisotropy expected from the Galactic CG effect. The width of the vertical color bin is 7.25 × 10^{-4} for the relative intensity in (A). The 1D projection is in map (**B**) for Dec between 25° and 70°, where the dashed line is the expected Galactic CG response and the solid line is the best fit to this observation using a first-order harmonic function. The fitting function is in the form of Amp × cos(R.A. – φ) where φ is in degrees and Amp is the amplitude. The χ^2 fit involves the ndf given by the number of bins minus two for the two fitting parameters Amp and φ. The data shows no Galactic CG effect with a confidence level of ~5 SD.

References and Notes

1. H. J. Voelk, in *Frontiers of Cosmic Ray Science*, T. Kajita, Y. Asaoka, A. Kawachi, Y. Matsubara, M. Sasaki, Eds. (Universal Academy Press, Tokyo, 2003), pp. 29–48.
2. Y.-Q. Lou, *Astrophys. J.* **428**, L21 (1994).
3. A. Dar, *Nuovo Cim. B* **120**, 767 (2005).
4. C. Yu, Y.-Q. Lou, F. Y. Bian, Y. Wu, *Mon. Not. R. Astron. Soc.* **370**, 121 (2006).
5. A. D. Erlykin, A. W. Wolfendale, *Astropart. Phys.* **25**, 183 (2006).
6. G. F. Krymsky, *Geomagn. Aeron.* **977**, 763 (1964).
7. E. N. Parker, *Planet. Space Sci.* **13**, 9 (1965).
8. B. Heber, in *Proc. 27th Int. Cosmic Ray Conf.*, M. Simon, E. Lorenz, M. Pohl, Eds., Invited, Rapporteur and Highlighted papers (CDROM, 2002) pp. 118–135.
9. A. H. Compton, I. A. Getting, *Phys. Rev.* **47**, 817 (1935).
10. D. J. Cutler, D. E. Groom, *Nature* **322**, L434 (1986).
11. M. Amenomori *et al.*, *Phys. Rev. Lett.* **93**, 061101 (2004).
12. K. Nagashima, S. Mori, in *Proc. Int. Cosmic Ray Symp. on High Energy Cosmic Ray Modulation*, Univ. of Tokyo, Tokyo, Japan, 326 (1976).
13. K. Nagashima, K. Fujimoto, R. M. Jacklyn, *J. Geophys. Res.* **103**, 17429 (1998).
14. K. Munakata *et al.*, *Phys. Rev.* **D56**, 23 (1997).
15. M. Ambrosio *et al.*, *Phys. Rev.* **D67**, 042002 (2003).
16. M. Aglietta *et al.*, in *Proc. 28th Int. Cosmic Ray Conf.*, T. Kajita, Y. Asaoka, A. Kawachi, Y. Matsubara, M. Sasaki, Eds., (Universal Academy Press, Tokyo, 2003) **4**, pp. 183–186.
17. T. Antoni *et al.*, *Astrophys. J.* **604**, 687 (2004).
18. G. Guillian *et al.*, *Phys. Rev.* D, in press (see http://arxiv.org/astro-ph/0508468).
19. M. Amenomori *et al.*, *Astrophys. J.* **626**, L29 (2005).
20. D. L. Hall *et al.*, *J. Geophys. Res.* **103**, 367 (1998).
21. D. L. Hall *et al.*, *J. Geophys. Res.* **104**, 6737 (1999).
22. M. L. Duldig, *PASA* **18** (1), 12 (2001).
23. M. Amenomori *et al.*, *Phys. Rev. Lett.* **69**, 2468 (1992).
24. M. Amenomori *et al.*, in International Symposium on High Energy Gamma-Ray Astronomy, F. A. Aharonian, H. J. Voelk, Eds., *AIP Conf. Proc.* **558**, 557 (2001).
25. M. Amenomori *et al.*, in *Proc. 27th Int. Cosmic Ray Conf.*, M. Simon, E. Lorenz, M. Pohl, Eds. (Copernicus Gesellschaft, 2002), **2**, pp. 573–576.
26. M. Amenomori *et al.*, *Phys. Rev.* **D47**, 2675 (1993).
27. M. Amenomori *et al.*, *Astrophys. J.* **598**, 242 (2003).
28. M. Amenomori *et al.*, *Nucl. Instrum. Methods Phys. Res. A* **288**, 619 (1990).

29. K. Kasahara, http://cosmos.n.kanagawa-u.ac.jp/EPICSHome/.
30. M. Amenomori *et al.*, *Astrophys. J.* **633**, 1005 (2005).
31. F. A. Aharonian *et al.*, *A & A* **393**, L37 (2002).
32. S. D. Hunter *et al.*, *Astrophys. J.* **481**, 205 (1997).
33. R. Atkins *et al.*, *Phys. Rev. Lett.* **95**, 251103 (2005).
34. G. Walker, R. Atkins, D. Kieda, *Astrophys. J.* **614**, L93 (2004).
35. L. Bergamasco *et al.*, in *Proc. 21th Int. Cosmic Ray Conf. (Adelaide)*, **6**, 372–375 (1990).
36. E. N. Parker, *Astrophys. J.* **145**, 811 (1966).
37. Z. H. Fan, Y.-Q. Lou, *Nature* **383**, 800 (1996).
38. Y.-Q. Lou, Z. H. Fan, *Mon. Not. R. Astron. Soc.* **341**, 909 (2003).
39. Y.-Q. Lou, X. N. Bai, *Mon. Not. R. Astron. Soc.*, in press, astro-ph/0607328 (2006).
40. Unless otherwise stated, images in Figs. 1 to 4 are presented using pixels in a radius of 5° and are sampled over a square grid of side width 2°; the modal energy is 3 TeV.

41. The collaborative experiment of the Tibet Air Shower Arrays has been performed under the auspices of the Ministry of Science and Technology of China and the Ministry of Foreign Affairs of Japan. This work was supported in part by Grants-in-Aid for Scientific Research on Priority Areas (712) (MEXT), by the Japan Society for the Promotion of Science, by the National Natural Science Foundation of China, and by the Chinese Academy of Sciences. The authors thank J. Kóta for reading the manuscript and for critical comments.

23 June 2006; accepted 22 September 2006
10.1126/science.1131702

Isolated Single-Cycle Attosecond Pulses

G. Sansone,[1] E. Benedetti,[1] F. Calegari,[1] C. Vozzi,[1] L. Avaldi,[2] R. Flammini,[2] L. Poletto,[3] P. Villoresi,[3] C. Altucci,[4] R. Velotta,[4] S. Stagira,[1] S. De Silvestri,[1] M. Nisoli[1]*

We generated single-cycle isolated attosecond pulses around ~36 electron volts using phase-stabilized 5-femtosecond driving pulses with a modulated polarization state. Using a complete temporal characterization technique, we demonstrated the compression of the generated pulses for as low as 130 attoseconds, corresponding to less than 1.2 optical cycles. Numerical simulations of the generation process show that the carrier-envelope phase of the attosecond pulses is stable. The availability of single-cycle isolated attosecond pulses opens the way to a new regime in ultrafast physics, in which the strong-field electron dynamics in atoms and molecules is driven by the electric field of the attosecond pulses rather than by their intensity profile.

The past decade has seen remarkable advances in the field of femtosecond (1 fs = 10^{-15} s) light pulses with few optical cycles (*1*). The main achievements have been (i) the generation of ultrabroadband light pulses, directly from a laser oscillator or with the use of external spectral broadening mechanisms; (ii) the development of sophisticated techniques for dispersion compensation on ultrabroad bandwidths; (iii) the use of experimental methods for complete temporal characterization of ultrashort pulses, particularly frequency-resolved optical gating (FROG) (*2*) and spectral phase interferometry for direct electric field reconstruction (SPIDER) (*3*), in a number of different experimental implementations; and (iv) the generation of few-cycle light pulses with precisely controlled and reproducible electric field waveform [stabilized carrier-envelope phase (CEP)] (*4*–*6*). We show that these achievements can now be extended to the attosecond (1 as = 10^{-18} s) domain. We demonstrate the compression and the complete temporal characterization of isolated pulses with durations down to 130 as at 36-eV photon energy, which consist of less than 1.2 periods of the central frequency. This source of extreme ultraviolet (XUV) radiation lends itself as a tool to investigate basic electron processes in a spectral range approaching the energy level of the outermost electrons in atoms, molecules, and solid-state systems. The XUV source opens the way to a new regime in the applications of attosecond pulses in which a medium interacts with nearly single-cycle isolated attosecond pulses. Moreover, in this case it is appropriate to analyze the role of the CEP of the generated attosecond pulses. Using numerical simulations, we demonstrate that the carrier-envelope phase of the attosecond pulses is characterized by an excellent stability.

So far, isolated attosecond pulses with multiple optical cycles have been produced by selecting the high-energy (cut-off) harmonics (~90 eV) generated in neon by few-cycle (<7 fs) linearly polarized fundamental pulses with stabilized CEP (*7*–*9*). In this case, the minimum pulse duration of the XUV pulses is limited by the bandwidth of the selected cut-off harmonics (~10 eV), thus preventing the generation of single-cycle attosecond pulses. A different approach for the generation of broadband isolated attosecond pulses is based on the use of phase-stabilized few-cycle driving pulses in combination with the polarization gating technique (*10*–*13*). Such a method uses the strong dependence of the harmonic generation process on the ellipticity of the driving pulses in order to obtain a temporal window of linear polarization for the fundamental pulses. XUV generation is possible only during this temporal polarization gate, which can be shorter than half an optical cycle of the fundamental radiation. In combination with the use of few-cycle driving pulses with stable CEP, this technique allows the generation of broadband isolated attosecond pulses. The advantages of this method are (i) the generation of broadband XUV pulses; (ii) the broad tunability of the attosecond pulses upon changing the generating gas medium; (iii) energy scalability; and (iv) the possibility to access the single-cycle regime.

The generation of broadband attosecond pulses is an important tool for photoelectron spectroscopy. Although they are not Fourier limited (chirped pulses), broadband attosecond pulses can be used to measure attosecond electron dynamics just as effectively as if the pulses were transform limited (*14*). However, in this case a complete temporal characterization of the attosecond pulses is required. On the other hand, for a number of applications in which the temporal structure of the attosecond pulses is important, dispersion compensation is required in order to obtain pulses with duration close to the transform-limited value. To completely characterize the attosecond pulses in terms of temporal intensity and phase, we experimentally applied the method of FROG for complete reconstruction of attosecond burst (FROG CRAB, hereafter called CRAB) (*15*), an extension to attosecond electron wavepackets of the FROG method. When an atom is ionized by an XUV attosecond electric field in the presence of a streaking infrared (IR) pulse, the IR electric field acts as an ultrafast phase modulator on the generated electron wavepacket. The corresponding photo-ionization spectrum can be written as a FROG spectrogram with a pure phase gate $\phi(t)$ (*15*):

$$\phi(t) = -\int_t^{\infty} dt'[\mathbf{v}\cdot\mathbf{A}(t') + \mathbf{A}^2(t')/2] \quad (1)$$

where $\mathbf{A}(t)$ is the vector potential of the IR field and $\mathbf{v}$ is the final electron velocity. A number of iterative algorithms can then be used to reconstruct the electric field of both the attosecond pulse and of the streaking IR pulse from the measured CRAB trace.

[1]National Laboratory for Ultrafast and Ultraintense Optical Science–CNR-Istituto Nazionale per la Fisica della Materia, Department of Physics, Politecnico, Piazza Leonardo da Vinci 32, 20133 Milano, Italy. [2]CNR-Istituto di Metodologie Inorganiche e dei Plasmi Area della Ricerca di Roma 1, Monterotondo Scalo 00016, Italy. [3]Laboratory for Ultraviolet and X-ray Optical Research–CNR-INFM, Department of Information Engineering–Università di Padova, Padova 35131, Italy. [4]Consorzio Nazionale Interuniversitario per le Scienze Fisiche della Materia-Dipartimento di Scienze Fisiche, Università di Napoli Federico II, Napoli 80138, Italy.

*To whom correspondence should be addressed. E-mail: mauro.nisoli@fisi.polimi.it